Received: 19 January 2024 | Revised: 12 April 2024 | Accepted: 10 June 2024

DOI: 10.1111/pce.15011

ORIGINAL ARTICLE

Plant, Cell & Environment

WILEY

Hyperspectral signals in the soil: Plant–soil hydraulic connection and disequilibrium as mechanisms of drought tolerance and rapid recovery

Yangyang Song[1] | Gerard Sapes[1] | Spencer Chang[2] | Ritesh Chowdhry[2] | Tomas Mejia[2] | Anna Hampton[2] | Shelby Kucharski[3] | T. M. Shahiar Sazzad[2] | Yuxuan Zhang[2] | Barry L. Tillman[4] | Márcio F. R. Resende Jr[5] | Sanjeev Koppal[2] | Chris Wilson[1] | Stefan Gerber[6] | Alina Zare[2] | William M. Hammond[1]

[1]Agronomy Department, University of Florida, Gainesville, Florida, USA

[2]Department of Electrical and Computer Engineering, University of Florida, Gainesville, Florida, USA

[3]School of Natural Resources and Environment, University of Florida, Gainesville, Florida, USA

[4]North Florida Research and Education Center, University of Florida, Marianna, Florida, USA

[5]Horticultural Sciences Department, University of Florida, Gainesville, Florida, USA

[6]Soil, Water and Ecosystem Sciences Department, University of Florida, Gainesville, Florida, USA

Correspondence
Yangyang Song and William M. Hammond, Agronomy Department, University of Florida, Gainesville, FL, USA.
Email: yangyangsong2015@outlook.com and Email: williamhammond@ufl.edu.

Alina Zare, Department of Electrical and Computer Engineering, University of Florida, Gainesville, FL, USA.
Email: azare@eng.ufl.edu

Funding information
Florida Peanut Producers Association; Southeastern Peanut Research Initiative; National Institute of Food and Agriculture; U.S. Department of Agriculture

Abstract

Predicting soil water status remotely is appealing due to its low cost and large-scale application. During drought, plants can disconnect from the soil, causing disequilibrium between soil and plant water potentials at pre-dawn. The impact of this disequilibrium on plant drought response and recovery is not well understood, potentially complicating soil water status predictions from plant spectral reflectance. This study aimed to quantify drought-induced disequilibrium, evaluate plant responses and recovery, and determine the potential for predicting soil water status from plant spectral reflectance. Two species were tested: sweet corn (*Zea mays*), which disconnected from the soil during intense drought, and peanut (*Arachis hypogaea*), which did not. Sweet corn's hydraulic disconnection led to an extended 'hydrated' phase, but its recovery was slower than peanut's, which remained connected to the soil even at lower water potentials (−5 MPa). Leaf hyperspectral reflectance successfully predicted the soil water status of peanut consistently, but only until disequilibrium occurred in sweet corn. Our results reveal different hydraulic strategies for plants coping with extreme drought and provide the first example of using spectral reflectance to quantify rhizosphere water status, emphasizing the need for species-specific considerations in soil water status predictions from canopy reflectance.

KEYWORDS

drought, hyperspectral reflectance, pre-dawn disequilibrium, recovery, rhizosphere

1 | INTRODUCTION

Drought poses a substantial and escalating threat to global crop production and survival (Dwivedi et al., 2018). Climate change-induced droughts and heatwaves have the potential to intensify one another (Mickelbart et al., 2015), leading to more frequent and severe droughts (Alizadeh et al., 2020; Legg, 2021), and to escalating risk of their especially dangerous combination, so-called 'hotter-drought' (Hammond et al., 2022). Edaphic drought (i.e., soil-related), in particular, will significantly threaten the productivity of dryland areas covering approximately 41% of the Earth's land surface, which provides food security for over 38% of the global population (Reynolds et al., 2007). While various studies have detailed the physiological responses of aboveground plant organs to edaphic drought (Fàbregas & Fernie, 2019; Gupta et al., 2020), and although scientists succeed in assessing soil water status during edaphic droughts (Whalley et al., 2013; Ma et al., 2019), monitoring water status at the root–soil interface remains challenging. Notably, plants can become disconnected from the drying soil (Duddek et al., 2022), resulting in a pre-dawn disequilibrium in water potentials between soil and plant. Thus, to better understand the incoming droughts on plant growth and survival, we need a comprehensive understanding of plant drought responses and recovery, along with high-throughput methods to assess plant water status, particularly focusing on the root–soil interface.

Edaphic droughts directly affect the soil–plant–atmosphere continuum upon which plant productivity and growth depend. The soil–plant–atmosphere continuum allows water movement from the soil through the plant vascular system to the atmosphere following a declining water potential gradient (Elfving et al., 1972). During drought, plants close stomata to reduce water loss, decreasing transpiration and photosynthesis (Martin-StPaul et al., 2017; Scoffoni & Sack, 2017). As drought intensifies, increased tension can induce emboli formation in xylem conduits. Embolism of distal organs (e.g., leaves, fine roots) may cause hydraulic segmentation and act as a 'hydraulic fuse', to limit the tension and embolism formation in the xylem of proximal organs (Cuneo et al., 2016; Michaletz, 2018; Wolfe et al., 2016). The embolized xylem impedes water transport and ultimately leads to distal organ death (McDowell et al., 2022) but reduces the risk of death in more proximal organs from which plants can often resprout (e.g., main stem, coarse roots). Pre-dawn leaf water potential (Ψ_{pd}) is widely used as a proxy of soil water potential (Ψ_{soil}) as the water potentials of leaves and soil are assumed to equilibrate overnight in the absence of transpiration (Li et al., 2019; Samuelson et al., 2014). However, despite this broad assumption about plant–soil equilibrium before daily transpiration, pre-dawn disequilibrium has been documented to occur in various plant species (Donovan et al., 1999, 2001, 2003; Groenveld et al., 2023; Scholz et al., 2007). This disequilibrium has been attributed to factors such as night-time transpiration, accumulation of apoplastic solutes in leaves, and a failure to restore tissue capacitance during the night (Bucci et al., 2004; Cavender-Bares et al., 2007). Disequilibrium can also occur when soil undergoes drying, with the initial response being root hair shrinkage, progressing to the formation of cortical lacunae, fine root mortality and subsequent coarse root shrinkage (Cuneo et al., 2016; Duddek et al., 2022). Additionally, root exudates such as mucilage may enhance water retention in the rhizosphere compared to the surrounding soil during drying (Carminati, 2012). These mechanisms might serve to prevent plant exposure to potentially lethal soil water potentials. Because plant and soil water potential at pre-dawn can become decoupled, Ψ_{pd} can mechanistically serve as the parameter to assess the degree of decoupling during drought. Such decoupling should increase over the course of a severe drought and may dictate recovery rates. However, pre-dawn disequilibrium studies have been primarily conducted under well-watered or mild drought conditions (Donovan et al., 1999, 2001; Groenveld et al., 2023). A comprehensive evaluation of plants transitioning from well-watered conditions to severe drought could provide a more thorough understanding of the connection between plant and soil water status and reveal when disequilibrium occurs, and why.

Direct measurements of plant water status have predominantly focused on above-ground tissues, while monitoring root water status has been limited due to the difficulty in accessing roots (Chang et al., 2023). Commonly used leaf water status metrics include leaf equivalent water thickness (EWT), relative water content (RWC), and leaf water potential (Ψ_{leaf}). The EWT, calculated as the absolute water content per leaf area unit, serves as an indicator of overall plant drought conditions (Xu et al., 2020). The RWC reflects the overall plant water balance and indicates leaf cell volume shrinkage (Martinez-Vilalta et al., 2019; Sack et al., 2018). The Ψ_{leaf} represents the driving force of water movement and is used to document critical physiological states, including the point of stomatal closure, bulk turgor loss, and hydraulic failure (Bartlett et al., 2012; Hammond et al., 2019; Rodriguez-Dominguez et al., 2022). Water potential and RWC could also be used to assess root water status. However, traditional measurements of plant RWC or water potential require either extensive tissue excision or the use of a pressure chamber or psychrometers, limiting their application to small-scale or low-throughput assessments. The advancement of real-time spectral prediction techniques enables the continuous and noninvasive assessment of leaf water status, such as leaf EWT (Féret et al., 2019), leaf RWC (Ihuoma & Madramootoo, 2019) and the turgor loss point (Castillo-Argaez et al., 2024). However, recent root imaging technologies, such as digging out and imaging (Le Bot et al., 2010; Shen et al., 2020), magnetic resonance imaging (Haber-Pohlmeier et al., 2019; Pflugfelder et al., 2017), minirhizotron (MR) systems (Gloaguen et al., 2019; Zurweller et al., 2018) and rhizoboxes (Gloaguen et al., 2022; Song et al., 2021), have primarily focused on root phenology and structure, including rooting depth, root length, root surface area and root volume. Among the various options, for field studies of root water status, the MR system would be ideal if appropriate spectral reflectance sensing technology could be developed. However, no existing study has identified wavelengths important for predicting soil and root water status, which are critical for developing a multi- or hyperpectral MR system. A standard MR system consists of an imaging station and an RGB camera equipped with an LED light, which moves within a transparent tube inserted underground, enabling continuous and noninvasive monitoring of roots.

With the appropriate lighting and identification of the critically important wavelengths to predict root and soil water status, this system could enable functional insights on the soil–root interface during edaphic droughts, similar to recent advances made in the spectral ecophysiology of leaves (Castillo-Argaez et al., 2024).

One critical challenge for assessing pre-dawn disequilibrium is the difficulty in directly sensing the water status of roots and soil, especially at the plant–soil interface. Plant spectroscopy could potentially be used to predict plant and rhizosphere water status in high-frequency and nondestructively due to its success in sensing many traits and states of plants and soil. For example, hyperspectral reflectance can predict plant stress, health, and chemistry, including foliar nutrients (Grieco et al., 2022), pigment composition (Blackburn et al., 2007) and vegetation water content (Hanavan et al., 2015), as well as soil organic carbon (Bangelesa et al., 2020), soil water content (Babaeian et al., 2015) and soil nutrients (Guo et al., 2021). Reflectance has been used to monitor leaf and canopy water status using spectral indices that use a few specific wavelengths (Sapes et al., 2024). However, the belowground organs remain unexplored when sensing plant–soil water relations. While some studies have used the whole visible (VIS) to shortwave infrared (SWIR) range (hyperspectral reflectance) to phenotype root morphology and structure (Bodner et al., 2018; Narisetti et al., 2021), predicting root water status remains a serious challenge. Using hyperspectral reflectance imaging during plant dehydration and rehydration could provide a more comprehensive understanding of water status, considering that both water content and water potential could potentially serve as reliable indicators of plant water status (Xu et al., 2020) and that hyperspectral reflectance imaging provides spatially explicit information.

Here, we investigate the response and recovery of *Arachis hypogaea* L. (peanut) and *Zea mays* (sweetcorn) during an experiment of extreme drought and recovery while they are growing in rhizoboxes accessible for hyperspectral imaging above- and below-ground. Peanuts and sweetcorn were chosen to represent C3 and C4 species and varying leaf phenology. We develop spectral models for leaf, root and soil water status capable of predicting water potential disequilibrium and identified crucial spectral signals associated with plant and soil water status. We designed our study to test the following three hypotheses:

1. Severe drought conditions will lead to pre-dawn water potential disequilibrium between plant and soil water status.
2. Spectral reflectance can accurately predict the water status of plant organs and soil.
3. Leaf spectral reflectance will be a good predictor of soil water status until disequilibrium occurs.

2 | MATERIALS AND METHODS

2.1 | Rhizobox construction

Plants were planted as seeds and cultivated in rhizoboxes ($L \times W \times D$: 34.5 × 21 × 3.8 cm). The choice of rhizobox dimensions was restricted to the hyperspectral camera's focal depth, and the available space in the dark imaging booth. Although this relatively small volume could impact plant root development, the dimensions of all rhizoboxes were rigorously controlled to ensure uniform effects across all plants. The rhizobox was made of black lightproof plastic on the bottom and three sides of the body. The fourth side was made of a transparent polycarbonate resin sheet (Lexan®, $L \times W$: 35.5 × 21.5 cm) to visualize root growth and development. Foam weatherstripping was placed between the plastic edge and Lexan sheet and the plastic boxes. In addition, all edges and screws used for constructing the rhizobox were sealed with black opaque liquid electrical tape as a sealant to prevent water leaks. Three drainage holes were made on the bottom of the rhizobox to allow water drainage, and a piece of 400 mesh (37 µm) screen placed inside the box covered these holes to prevent soil loss during irrigation. The top of each rhizobox was covered using transparent plastic cling wrap to reduce water loss from evaporation; drain holes at the bottom of the boxes were left uncovered to prevent inundation during watering. The growing medium for this experiment was a fritted calcined clay, Profile Porous Ceramic (Greens Grade™; Turface Athletics), hereafter referred to as 'soil'. We filled each rhizobox with approximately 1500 g of soil and over-irrigated, drip-dried and weighed them multiple times to ensure the soil in each box reached its saturation point. The weights of dry soil and saturated soil were recorded.

2.2 | Experiment design and treatment

Experiments were carried out using two plant species, peanut (*Arachis hypogaea* L.) and sweet corn (*Zea mays* L.). Two sweet corn lines, IL4H/S213531 and IL395a/S213532, and peanut genotype TUFRunner™ '511' (Tillman & Gorbet, 2017) and line 10 × 34-4-4-1-2, were grown in 64 rhizoboxes, with 16 boxes per genotype. One seed per box for sweet corn and peanut was sown on 19 and 26 May 2022, respectively. During the experiment, each rhizobox was kept in an opaque white bubble-padded envelope (lightproof) to minimize physical scratches on the Lexan sheet and reduce the effects of light interference and temperature fluctuation on root growth. Groups of 10 rhizoboxes were arranged in containers and placed on a greenhouse bench. Each container was placed on a wooden table easel inclined at a 30° angle, with the transparent side of all the rhizoboxes facing down. This ensured that roots would grow against the transparent sheet following gravitropism (Gloaguen et al., 2022). Temperatures ranged between 16°C and 33°C and relative humidity ranged between 70% and 85% based on greenhouse environmental control settings. Light reaches ~1200 Umol m^{-2} s^{-1} of photosynthetic photon flux density (PPFD) during full sun exposure. Once the seedling emerged, a small hole was made in the plastic cling wrap at the top of the rhizobox to allow the upward growth of the shoot unimpeded. After emergence, we top-dressed each rhizobox with one scoopful controlled-release fertilizer 'osmocote' (Osmocote, 15:9:12 N–P–K; The Scotts Company), so that the fertilizer would not be in the soil but able to leach nutrients during watering. Additionally, 1 L of water

(Supporting Information S1: Figure 1, approximately 1 L water saturated the soil in each box) was added to each box daily until 41 days after planting (DAP) for sweet corn and 78 DAP for peanut, respectively (Figure 1). After which, we stopped the irrigation for 11 rhizoboxes per genotype to initiate dehydration and the other five rhizoboxes served as reference for well-watered plants (Figure 1). During dehydration, 1-2 rhizobox were sampled for destructive measurements of plant leaf, stem, root and soil when the Ψ_{pd} reached 0 to −0.5 (Ψ_1), −0.5 to −1.0 (Ψ_2), −1.0 to −1.5 (Ψ_3), −1.5 to −2.0 (Ψ_4) and −2.0 to −3.0 (Ψ_5) MPa for sweet corn and reached around 0 to −1.0 (Ψ_1), −1.0 to −2.0 (Ψ_2), −2.0 to −3.0 (Ψ_3), −3.0 to −4.0 (Ψ_4) and < −4.0 (Ψ_5) MPa for peanut (Figure 1). The water supply (1 L per box daily) resumed at 70 and 91 DAP until the end of the experiment (75 and 96 DAP) for sweet corn and peanut, respectively (Figure 1). The other five drought-treated rhizoboxes per crop species were used to assess drought recovery after rehydration (Figure 1).

2.3 | Data collection

Plant physiological measurements were taken for the plants in each rhizobox. All plants were carefully transported from the greenhouse to the lab (where temperature was maintained at 22°C) at 4:30 AM to ensure the plants were well dark-adapted. We first measured the chlorophyll fluorescence to assess plant health and function during dehydration. Measurements were taken on a fully expanded peanut leaf on (or close to) the second node from the apex or the newly mature sweet corn leaf using an Imaging-PAM (Walz). The maximum potential quantum efficiency of Photosystem II (F_v/F_m) was obtained by averaging the F_v/F_m values of the imaged leaf area. Following the F_v/F_m measurements, we removed one mature and healthy leaf per box to measure Ψ_{pd} with a Scholander pressure chamber (model 1505D-EXP; PMS Instrument) by gradually increasing the pressure at a rate of 0.01 MPa s^{-1} until the meniscus of the xylem sap was VIS at the cut surface (Bitterlich et al., 2018). After the water potential measurement, we determined the RWC of the same leaf using the following formula:

$$\mathrm{RWC} = \frac{\text{freshweight} - \text{dryweight}}{\text{saturatedweight} - \text{dryweight}} \times 100.$$

We weighed the fresh leaf and then measured the leaf area by using a leaf area metre (Li-Cor 3000; Li-Cor BioSciences). To obtain saturated weight, we submerged the leaf petiole in tap water for 2 h (Zwieniecki et al., 2007) for corn and 16 h for peanut, respectively, in the dark at 4°C to prevent oversaturation artifacts resulting from low osmotic potential due to starch conversion into sugars (Boyer et al., 2008). The rehydration time for a peanut leaf was obtained from a full rehydration curve

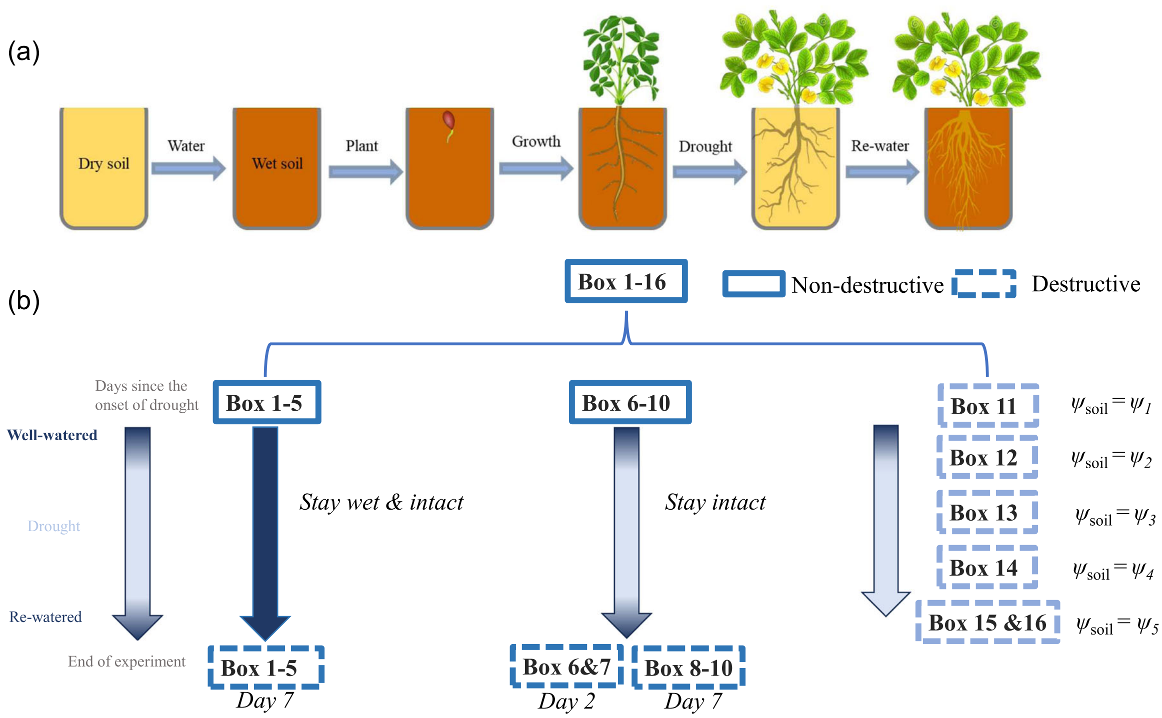

FIGURE 1 Illustration of the experiment design, using peanut genotype TUFRunner™ '511' as an example. (a) The process of the experiment, (hyper)spectral imaging and physiological measurements initiated on the first day of drought were applied until the end of the experiment. (b) The treatments applied to boxes; boxes 1–5 received full irrigation and were destructed on the last day of the experiment, serving as the controlled reference group. Intact boxes 6–10 experienced drought, and were destructively harvested for validation data on Day 2 and Day 7 after being rewatered. Boxes 11–16 experienced drought and were destructively harvested for validation data on the day when the soil water potential reached specific values ranging from wettest to driest. [Color figure can be viewed at wileyonlinelibrary.com]

(Supporting Information S1: Figure 2). After recording the saturated weight, each leaf was oven-dried at 70°C for at least 48 h, when mass became stable, to get the dry weight. Leaf EWT was calculated as

$$\mathrm{EWT} = \frac{\text{freshweight} - \text{dryweight}}{\text{leafarea}}.$$

One leaf of each plant was carefully wrapped in aluminium foil and enclosed in a plastic zip-lock bag the evening before measurements. The leaf water potential of the bagged leaf was measured to represent stem water potential (Ψ_{stem}, Tomasella et al., 2023). We conducted leaf spectra measurements on a fully expanded mature leaf using a spectroradiometer (HR-1024 spectroradiometer; SVC Corp.) with a wavelength range from 350 to 2500 and a spectral resolution of 1 nm. We trimmed the wavelength range to 400-2400 for model building to remove noisy bands at the edge of the sensor range. Leaf gas exchange was measured on four drought-treated and three well-watered plants per species from 8 AM to 12 PM at each sampling date. Net photosynthesis (A_{net}; μmol m^{-2} s^{-1}), stomatal conductance (g_s; mol m^{-2} s^{-1}) and transpiration (E; mmol m^{-2} s^{-1}) were measured on fully expanded mature leaves using an infrared gas analyzer (Li-Cor 6800; Li-Cor BioSciences). Measurements were conducted at a standardized PPFD of 1000 μmol m^{-2} s^{-1}. This value falls within the observed maximum PPFD range inside the greenhouse, which typically reaches up to 1200 μmol m^{-2} s^{-1}. Concurrently, the chamber maintained a reference CO_2 of 415 μmol s^{-1} at a temperature of 25°C. Leaf-to-air vapour pressure deficit (VPD) was maintained at levels between 1.0 and 2.0 kPa. Each leaf was given approximately 15 min to equilibrate before measurements were taken. The stability criteria (slope limit: 0.1 and standard deviation limit: 0.1) of sample CO_2 were also used to determine the timing of data logging. Daily measurements were taken on one leaf from each plant until drought-induced stomatal closure (i.e., g_s was reduced by >90%) on the dehydrating plants. After rehydration, leaf gas exchange was measured on five drought-treated and three well-watered plants at each sampling date.

We imaged each rhizobox to get the hyperspectral reflectance of roots in the soil. Each Rhizobox was imaged using a Hyperspectral Imager (model 4200; HinaLea Imaging). This camera has a wavelength range from 400 to 1000 nm with a spectral resolution of 2 nm. The imaged area was 8 cm × 15 cm, with a camera working distance of 1 m. The spectral reflectance of roots and soil was obtained through segmentation by a pretrained, deep convolutional learning model called ‘CubeNET’. The model was trained within the wavelength range of 450–926 nm using a subset of approximately 45 peanut root images from the HyperPRI data set (Chang et al., 2023). The hyperspectral cubes were fed into the model, and for each, we averaged the spectral signatures for pixels that were predicted as root and as soil. To remove noisy bands at the limits of sensor detection, we trimmed the wavelength range to 450–900 nm. Lastly, we destructively harvested two rhizoboxes, immediately collecting root samples and four soil samples per rhizobox from the hyperspectral imaging area to determine soil and root water potential (Ψ_{soil} and Ψ_{root}). Four soil samples per rhizobox were collected using steel caps (METER Group Inc.) which were placed in a WP4C dew-point Potentiometer to measure Ψ_{soil} (METER Group Inc.). We measured Ψ_{root} using a Scholander pressure chamber by carefully excavating and excising an intact secondary root and inserting it into the pressure chamber with the cut end facing upwards immediately after dismantling the rhizobox. Subsequently, we gradually increased the pressure at a rate of 0.01 MPa s^{-1} until the meniscus of the xylem sap became VIS at the cut surface (Bitterlich et al., 2018), the balancing pressure at this point was multiplied by −1, and recorded as $\Psi_{root.}$

2.4 | Statistical analysis

Statistical analyses were performed in R (version 4.2.2; R Core Team, 2020). Because we did not observe significant genotypic differences ($p < 0.05$) for both sweet corn and peanut, we deemed differences among genotypes to be scientifically trivial and therefore chose to pool data among genotypes within a species. Two-way analysis of variance (ANOVA) was used to test the significance of treatment effects at $p < 0.05$ level, followed by a Tukey honest significant difference post hoc analysis. For each species, we compared F_v/F_m, Ψ_{pd} and leaf RWC and EWT between well-watered and drought-treated plants among sampling days. We also assessed the differences among leaf, stem, root and soil pre-dawn water potential within each species on the driest day using one-way ANOVA. Trait values were presented as mean ± standard errors in the text.

Partial least square regression (PLSR, R package ‘pls’) was performed to develop a predictive model of plant and soil water status using spectral reflectance. The PLSR models were performed on three data sets: the sweet corn data set (n = 183 for leaf and n = 161 for root and soil), peanut data set (n = 154 for leaf and n = 134 for soil and root) and the combined data set (n = 337 for leaf and n = 295 for soil and root) of sweetcorn and peanut. Before model training, a representative 20% of the data was set aside using the kennard-stone algorithm (R package ‘prospectr’) which ensures even sampling across the range and distribution of a target variable. The 80% left was used for training and testing. The training and testing process used an iterative method with 100 iterations. Briefly, each iteration randomly divided the training and testing data set into two groups. The two groups were generated using a stratified octile sampling where data within each octile of the distribution was randomly allocated 80% into training and 20% into testing. This method ensured even sampling across the whole distribution of values within each iteration, which is important when data is not evenly distributed across the whole range of values. Within each iteration, the training subset was used to build a PLSR model. This model was then validated against the testing group and its performance was assessed based on root mean square error of prediction in percentage (%RMSE), R^2, slope and bias. The leaf spectral reflectance ranging from 400 to 2400 nm at a resolution of 1 nm was first used to develop PLSR models to predict Ψ_{pd}, leaf RWC and leaf EWT. To compare models and wavelength importance (using 'varImp' in R package 'caret') among leaf, root and soil, a second set of PLSR models was built using leaf spectra reflectance trimmed to 450–900 nm with a spectra resolution of 2 nm to meet the settings of the hyperspectral reflectance camera. The PLSR models based on spectral reflectance ranging from 450 to 900 nm were performed to predict leaf, root and soil water status. We have used Ψ_{pd} to represent Ψ_{root} and Ψ_{soil} in this data set under the assumption that hydraulic equilibrium happened among plant organs and soil. Data sets of estimated Ψ_{root} and Ψ_{soil} (Ψ_{pd} *estimated)* and corresponding spectral reflectance served as internal training and testing data sets. Data sets consisted of measured Ψ_{root} and Ψ_{soil} from harvested rhizoboxes and corresponding spectral reflectance served as independent validation data sets. For each PLSR model, the number of components was determined by choosing the number that resulted in the smallest RMSE during training (Cohen et al., 2010). The 100 models resulting from the 100 iterations of training and testing were applied to the validation data set to validate model performance on data that was not involved in building the models. Models with high R^2, low %RMSE, low bias and a slope between measured and predicted values close to 1 were considered higher-performing models.

3 | RESULTS

3.1 | Physiological response during dehydration

At the beginning of dehydration (Day 0), all plants were well-watered. Both sweet corn and peanut leaves had high photosynthetic potential, with unstressed peanut leaf F_v/F_m being slightly higher than sweet corn (0.85 ± 0.003 vs. 0.78 ± 0.004, $p < 0.05$). Upon drought initiation, peanut plant tissues dried faster than sweet corn, as sweet corn reached 75% leaf RWC on Day 6 while peanut reached 75% leaf RWC on Day 4 (Figure 2c,f). As a result, sweet corn Ψ_{pd} declined much slower than peanut Ψ_{pd} and most plants maintained a Ψ_{pd} around −2.0 MPa (Figure 2b). However, peanut Ψ_{pd} kept declining during the entire drought period (11 days), and the average Ψ_{pd} reached a minimum of −4.0 MPa (Figure 2e). Both stressed sweet corn (Day 15 and Day 23) and peanut (Day 7 and Day 11) plants showed lower leaf F_v/F_m (absolute value 0.1 for sweet corn and 0.04 for peanut averaged across days) than well-watered plants ($p < 0.05$, Figure 2a,d), but sweet corn (Day 23) had a greater reduction in FvFm (0.107 vs. 0.053) than peanut ($p < 0.05$, Day 11). After rehydration, the Ψ_{pd} and leaf RWC of both sweet corn and peanut recovered, and

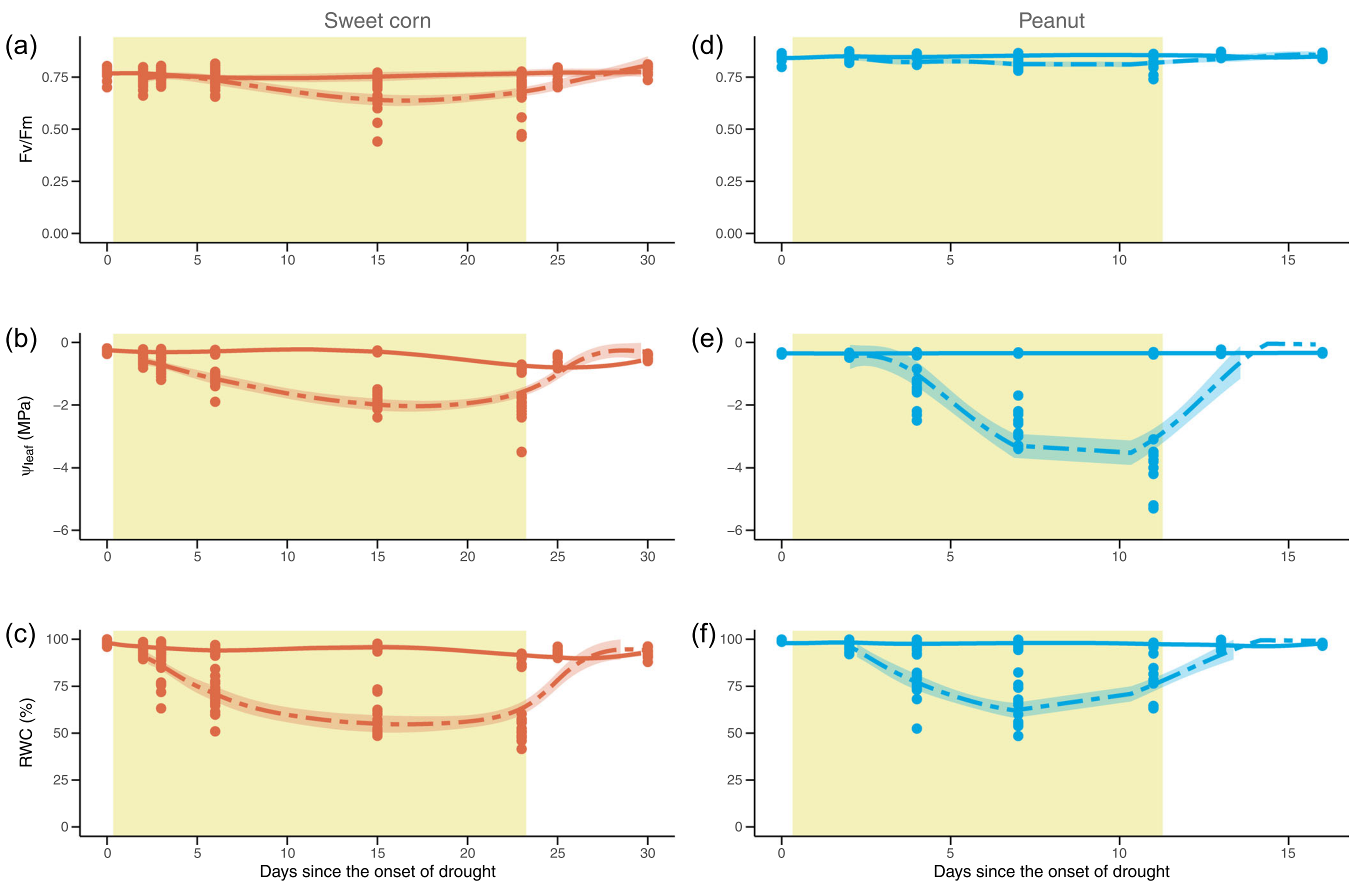

FIGURE 2 Plant leaf chlorophyll fluorescence, water potential (Ψ_{leaf}) and relative water content (RWC) of sweet corn (a–c) and peanut (d–f) during dehydration and rehydration. Dashed lines indicate plants that were subjected to drought and solid lines indicate plants that were well-watered, the yellow-shaded area in each panel refers to days that drought treatment was applied to the rhizoboxes shown by dashed lines. Regression lines in each panel are made using loess functions, and the 95% confidence interval is present as a shaded area around each regression line. [Color figure can be viewed at wileyonlinelibrary.com]

showed no differences compared with well-watered leaves, at 2 days after rewatering ($p < 0.05$, Figure 2b,c,e,f). However, sweet corn F_v/F_m recovered slower than peanut, with peanut showing no differences between rehydrated and control plants (0.85 ± 0.004 vs. 0.85 ± 0.002, $p < 0.05$, Figure 2d), while sweet corn showed lower F_v/F_m in rehydrated plants than control plants (0.74 ± 0.01 vs. 0.78 ± 0.009, $p < 0.05$, Figure 2a).

During the drought, peanut plants consistently maintained an F_v/F_m value greater than 0.75, while sweet corn experienced a steep decline after reaching a *Ψpd* of −1.0 MPa. F_v/F_m also reached a minimum of ~0.5 in sweet corn, near a hypothesized lethal limit of F_v/F_m for photosystems (Guadagno et al., 2017, Figure 3a). Sweet corn plants closed their stomata at *Ψpd* around −1.2 MPa, while peanut plants closed their stomata at Ψ_{pd} around −2.1 MPa (Figure 3c). The stomatal closure difference between sweet corn and peanut also led to the different A_{net} and transpiration rates between −1 and −2 MPa of Ψ_{pd}. ($p < 0.05$, Figure 3b,d).

3.2 | Pre-dawn disequilibrium

On the driest day of the drought -corresponding to Day 23 for sweet corn and Day 11 for peanut plants— we observed a pre-dawn disequilibrium between plant and soil water potential (Supporting Information S1: Figure 3, Figure 4). Sweet corn had Ψ_{pd}, Ψ_{stem} and Ψ_{root} at approximately −2.0 MPa, but the Ψ_{soil} was at −2.86 ± 0.08 MPa, significantly lower ($p < 0.05$) than all plant organs. This disequilibrium was not seen in peanut, which still had equilibrated water potentials even at Ψ_{soil} = −4.0 MPa.

3.3 | Leaf spectral reflectance (400–2400 nm) models for leaf water status

Leaf spectral reflectance provided varying estimates of leaf water status across organs and species (Table 1, Figure 5 and Supporting

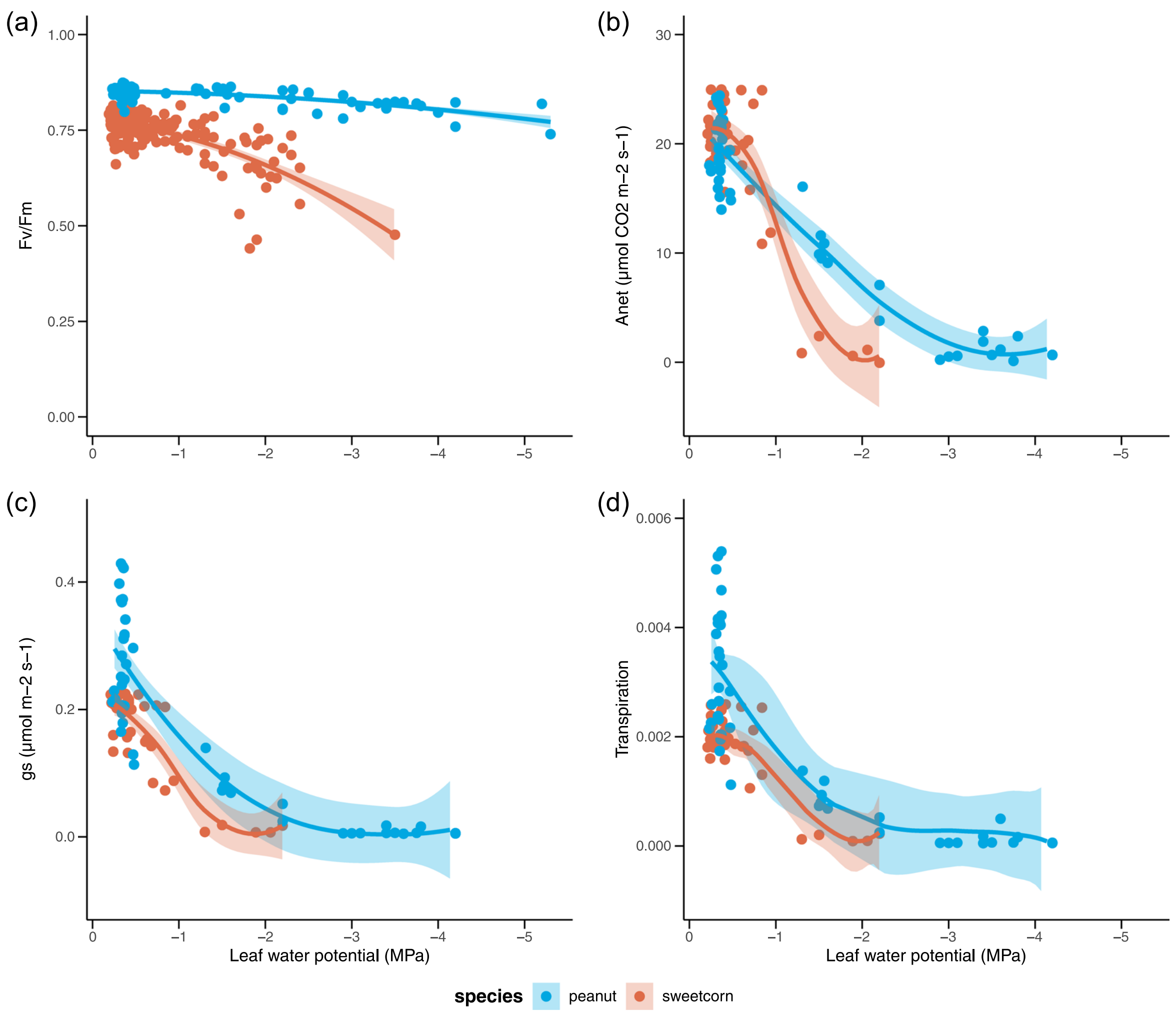

FIGURE 3 Plant dark-adapted chlorophyll fluorescence (F_v/F_m, a), net photosynthesis (A_{net}, b), stomatal conductance (g_s, c) and transpiration (E, d) of sweet corn (shown in red) and peanut (shown in blue) at different leaf water potentials. Regression lines in each panel are made using loess functions, and the 95% confidence interval is present as a shaded area around each regression line. [Color figure can be viewed at wileyonlinelibrary.com]

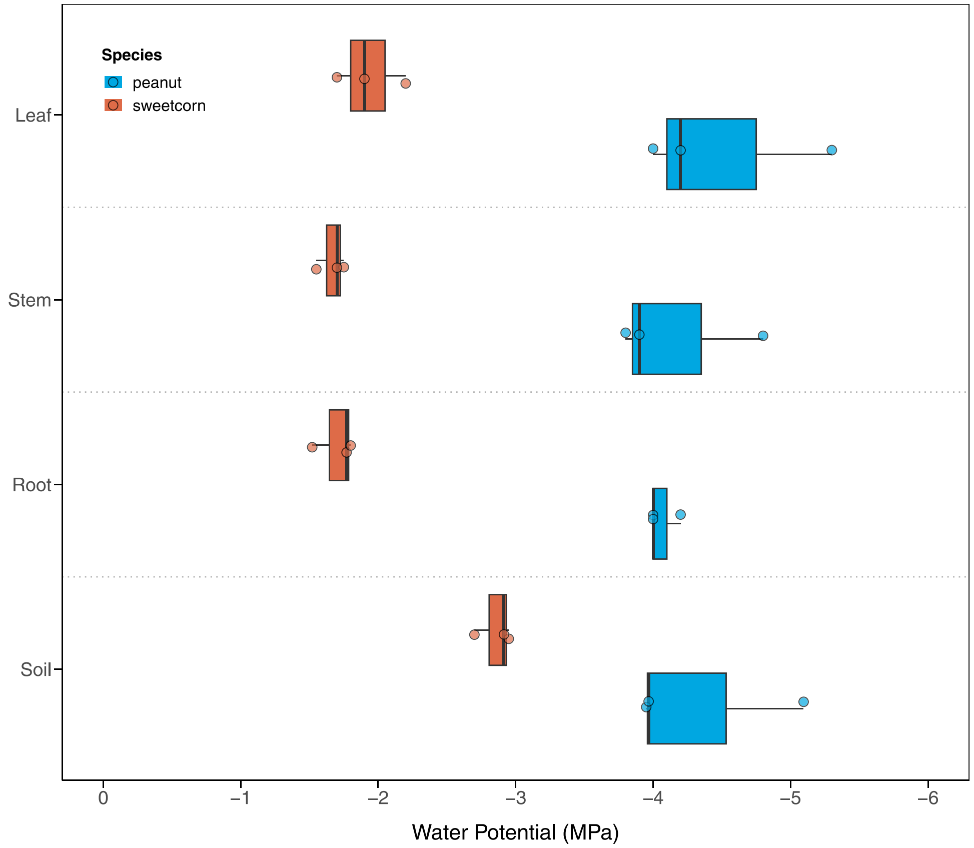

FIGURE 4 Water potentials of leaf, stem, root and soil of sweet corn (red boxplots) and peanut (blue boxplots) on the last day of drought treatment (e.g., at their most dehydrated state), taken from the destructively harvested validation boxes. Water potentials of sweet corn organs (leaf, stem and root, shown in red) were significantly higher than the soil water potential while water potentials among peanut organs (leaf, stem and root, shown in blue) and soil were not statistically different. [Color figure can be viewed at wileyonlinelibrary.com]

TABLE 1 Summary statistics for the models developed from internal training and testing data set for predicting leaf water status using spectral reflectance (full range, from 400 to 2400 nm) and applied to an external validation data set.

		Internal training and testing						External validation				
Species	Parameter	Components	Slope	%RMSE	Bias	R^2	*p* Value	Slope	%RMSE	Bias	R^2	*p* Value
Both species	Ψ_{leaf}	9	0.99	6.67	0.0054	0.82	<0.001	1.02	9.76	−0.1694	0.83	<0.001
	RWC	4	1.02	15.95	−0.3354	0.64	<0.001	0.87	21.44	−4.6961	0.55	<0.001
	EWT	5	0.98	11.52	0	0.75	<0.001	0.83	21.41	0.0014	0.35	<0.001
Sweet corn	Ψ_{leaf}	5	0.95	16.06	−0.0043	0.62	<0.001	0.88	16.2	−0.1726	0.61	<0.001
	RWC	2	1.03	17.36	0.2036	0.64	<0.001	0.75	25.27	−7.426	0.54	<0.001
	EWT	1	1.13	15.66	−0.0001	0.22	<0.001	1.36	26.01	0.0022	0.17	0.012
Peanut	Ψ_{leaf}	6	0.99	5.69	−0.0038	0.9	<0.001	1.04	12.91	−0.2368	0.83	<0.001
	RWC	6	0.99	12.31	−0.062	0.77	<0.001	1.01	19.83	−2.7035	0.61	<0.001
	EWT	4	1	9.09	0.0001	0.89	<0.001	1.1	9.37	−0.0002	0.9	<0.001

Abbreviations: EWT, equivalent water thickness; RWC, relative water content; %RMSE, root mean square error divided by 95% of trait range; Ψ_{leaf}, leaf water potential.

Information S1: Figure 4). Our peanut-based PLSR models achieved predictions for Ψ_{pd} ($R^2 = 0.9$, root mean square error of prediction [RMSEP] = 5.69%), RWC ($R^2 = 0.77$, RMSEP = 12.31%) and EWT ($R^2 = 0.89$, RMSEP = 9.09%). When applied to an independent data set, these models delivered predictions for Ψ_{pd} ($R^2 = 0.83$, RMSEP = 12.91%), RWC ($R^2 = 0.61$, RMSEP = 19.83%) and EWT ($R^2 = 0.9$, RMSEP = 9.37%) with intermediate to high accuracy.

Plant, Cell & Environment PC&E –WILEY

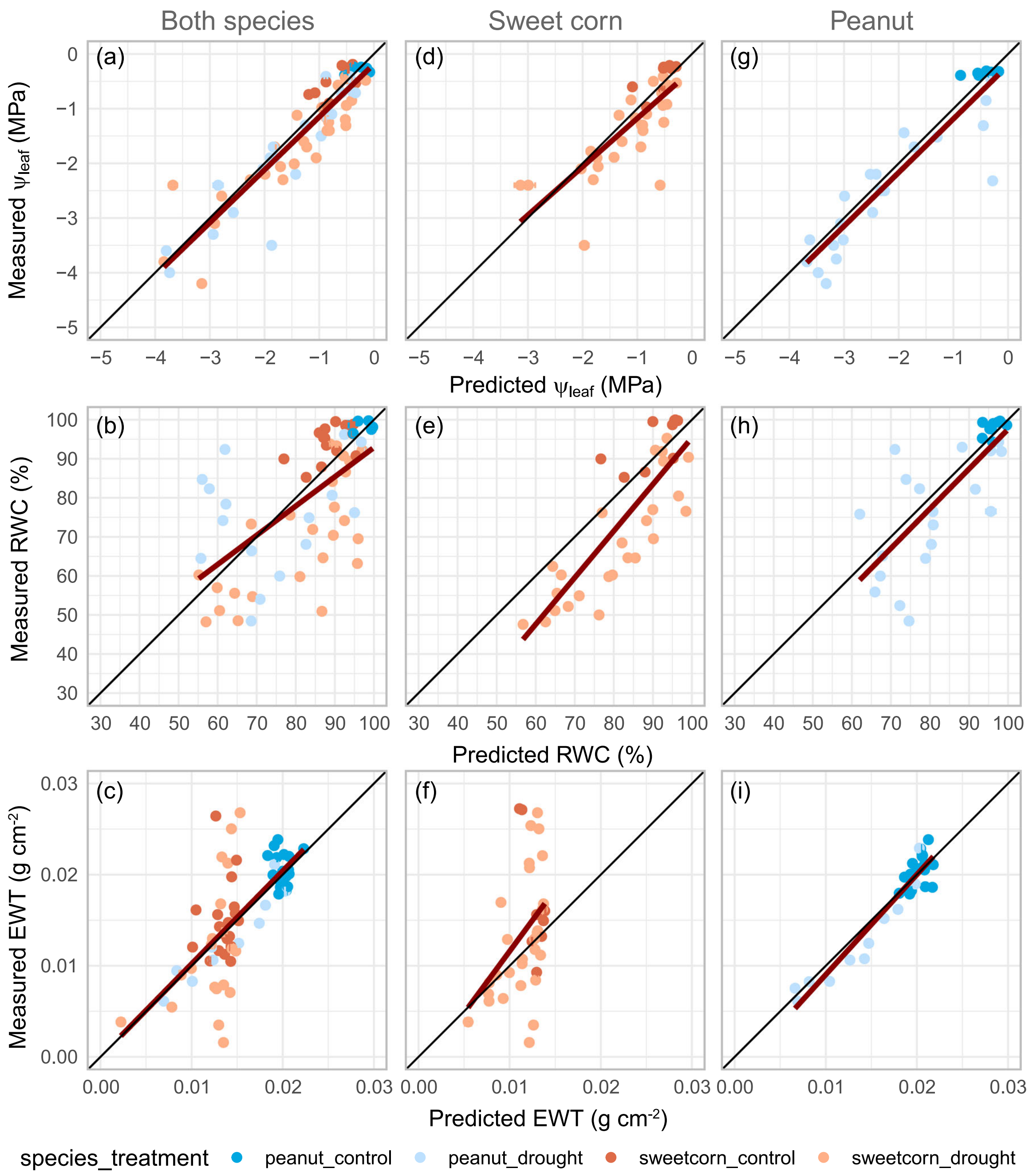

FIGURE 5 Plots of measured values against spectral reflectance (400–2400 nm) predicted values using partial least square regression on external validation data sets for leaf water potential (Ψ_{leaf}), relative water content (RWC) and equivalent water thickness (EWT) of pooled species (a–c), sweet corn (d–f) and peanut (g–i). Dark blue (red) points are from control (well-watered) plants, and light blue (red) points are from peanut (sweet corn) plants under drought treatment. The black line is the 1:1 line. The red line indicates the line of best fit using ordinary least squares for each panel. We applied models generated from 100 iterations during training and testing to the corresponding spectral reflectance to get the 95% confidence intervals of each point. [Color figure can be viewed at wileyonlinelibrary.com]

Conversely, PLSR models for sweet corn showed lower to intermediate accuracy in predicting Ψ_{pd} ($R^2 = 0.62$, RMSEP = 16.06%), RWC ($R^2 = 0.64$, RMSEP = 17.36%) and EWT ($R^2 = 0.22$, RMSEP = 15.66%). These models performed even less effectively ($R^2 = 0.17$–0.61, RMSEP = 16.02%–26.01%) when applied to an independent data set. When combining the peanut and sweet corn data sets, PLSR models showed intermediate to high accuracy for Ψ_{pd} ($R^2 = 0.82$, RMSEP = 6.67%), RWC ($R^2 = 0.64$, RMSEP = 15.95%) and EWT ($R^2 = 0.75$, RMSEP = 11.52%). On independent validation for pooled species data, Ψ_{pd} ($R^2 = 0.83$, RMSEP = 9.76%) and RWC ($R^2 = 0.55$, RMSEP = 21.44%) maintained intermediate to high accuracy, while EWT accuracy dropped significantly ($R^2 = 0.35$, RMSEP = 21.44%).

3.4 | Spectral reflectance (450–900 nm) models for leaf, root and soil water status

After trimming the leaf spectral reflectance to the 450–900 nm range to much the range of the sensor used for root and rhizosphere hyperspectral imaging, the PLSR model for Ψ_{pd}, developed from the peanut data set, retained high accuracy (R^2 = 0.88, RMSEP = 6.61%). In contrast, the PLSR models for Ψ_{pd}, developed from the sweet corn data set (R^2 = 0.5, RMSEP = 18.56%) and the pooled species data set (R^2 = 0.71, RMSEP = 8.52%), exhibited reduced accuracy (Table 2 and Supporting Information S1: Figure 5). Furthermore, we applied the PLSR models for Ψ_{pd} to three independent data sets, including peanut, sweet corn and pooled species. The models performed less effectively on these data sets compared to the internal training/testing (Table 2 and Figure 6, R^2 = 0.58–0.77, RMSEP = 14.82%–17.89%).

The PLSR models based on root and soil spectral reflectance also performed well. The PLSR models for Ψ_{root} and Ψ_{soil} of individual species demonstrated high accuracy (Table 2 and Supporting Information S1: Figure 5, R^2 = 0.78–0.9, RMSEP = 6.59%–10.13%). When species were pooled, the PLSR models for Ψ_{soil} maintained high accuracy (Table 2 and Supporting Information S1: Figure 5, R^2 = 0.8, RMSEP = 7.5%), while the PLSR models for Ψ_{root} lost accuracy (Table 2 and Supporting Information S1: Figure 5, R^2 = 0.57, RMSEP = 10.89%). The application of PLSR models for Ψ_{root} and Ψ_{soil} to the corresponding independent data sets yielded mostly intermediate to high accuracy (Table 2 and Figure 6, R^2 = 0.68–0.91, RMSEP = 12.58%–17.71%).

3.5 | Wavelength importance and similarities among plant organs and soil in visible and near-infrared range

The variable importance metric revealed broad similarities in the spectral regions (400–2400 nm) important for predicting leaf water status (Ψ_{pd}, RWC and EWT) across all three data sets (Supporting Information S1: Figure 6). Important wavelengths were the green bands at 550 nm, the red edge at 720 nm, as well as peaks around 1500 and 1800 nm in the SWIR region. The SWIR range from 750 to 1400 nm generally had greater importance in predicting peanut water status compared to sweet corn and the combined species (Supporting Information S1: Figure 6). When predicting Ψ_{pd} using the spectrum spanning from 450 to 900 nm, important wavelength ranges shared by all three data sets included peaks around 520 nm, the green bands at 550 nm, 630 nm, and the red edge spanning 670–720 nm.

The important wavelengths showed considerable variations when predicting peanut and sweet corn Ψ_{root} (Supporting Information S1: Figure 7). Wavelength bands in the 800–900 nm range were important for predicting peanut Ψ_{root}, while bands ranging from 450 to 625 nm were important for predicting sweet corn Ψ_{root}. Combining the peanut and sweet corn data sets, wavelength bands from 450 to 625 nm were important for predicting root water potential in both species. Important wavelengths for predicting peanut soil water potential included bands at 450, 520, and 575 nm, as well as several bands in the 680–900 nm range. For predicting sweet corn soil water potential, important wavelengths featured peaks at 520 nm and multiple peaks within the 680–900 nm range (Supporting Information S1: Figure 7). When combining the peanut and sweet corn data sets, important wavelengths for predicting soil water potential comprised peaks at 520, 580 and 740 nm (Supporting Information S1: Figure 7).

4 | DISCUSSION

Our models were able to predict leaf, root and soil water status from spectral reflectance over a range of water stress intensities in two species representing different drought response strategies. Even though the soil water potential significantly declined in both species, the hydraulic disequilibrium between soil and plant in the case of sweet corn indicated that plant canopy spectra alone would be

TABLE 2 Summary statistics for the models developed from internal training and testing data set for predicting plant organs water potential using spectral reflectance (VNIR, from 450 to 900 nm) and applied to an external validation data set.

		Internal training and testing						External validation				
Species	Parameter	Components	Slope	%RMSE	Bias	R^2	*p* Value	Slope	%RMSE	Bias	R^2	*p* Value
Both species	Ψ_{leaf}	7	0.99	8.52	0.0012	0.71	<0.001	0.86	14.82	−0.139	0.59	<0.001
	Ψ_{root}	6	0.94	10.89	−0.0086	0.67	<0.001	1.25	17.71	−0.3983	0.58	<0.001
	Ψ_{soil}	8	0.97	7.5	0.0038	0.8	<0.001	1.26	12.58	−0.1272	0.81	<0.001
Sweet corn	Ψ_{leaf}	7	0.91	18.56	−0.0144	0.58	<0.001	0.83	17.89	−0.2549	0.5	<0.001
	Ψ_{root}	7	1	8.6	0.0099	0.8	<0.001	0.89	14.69	−0.0072	0.84	<0.001
	Ψ_{soil}	5	0.98	6.99	−0.0017	0.87	<0.001	0.82	13.57	−0.0968	0.91	<0.001
Peanut	Ψ_{leaf}	9	1.06	6.61	−0.0037	0.88	<0.001	1.2	16.11	−0.3427	0.77	<0.001
	Ψ_{root}	4	0.99	10.13	−0.0061	0.78	<0.001	1.25	16.4	−0.2158	0.81	<0.001
	Ψ_{soil}	6	0.99	6.59	0.0104	0.9	<0.001	1.14	14.45	−0.2879	0.86	<0.001

Abbreviations: VNIR, visible and near-infrared range; %RMSE, root mean square error divided by 95% of trait range; Ψ_{leaf}, leaf water potential; Ψ_{root}, root water potential; Ψ_{soil}, soil water potential.

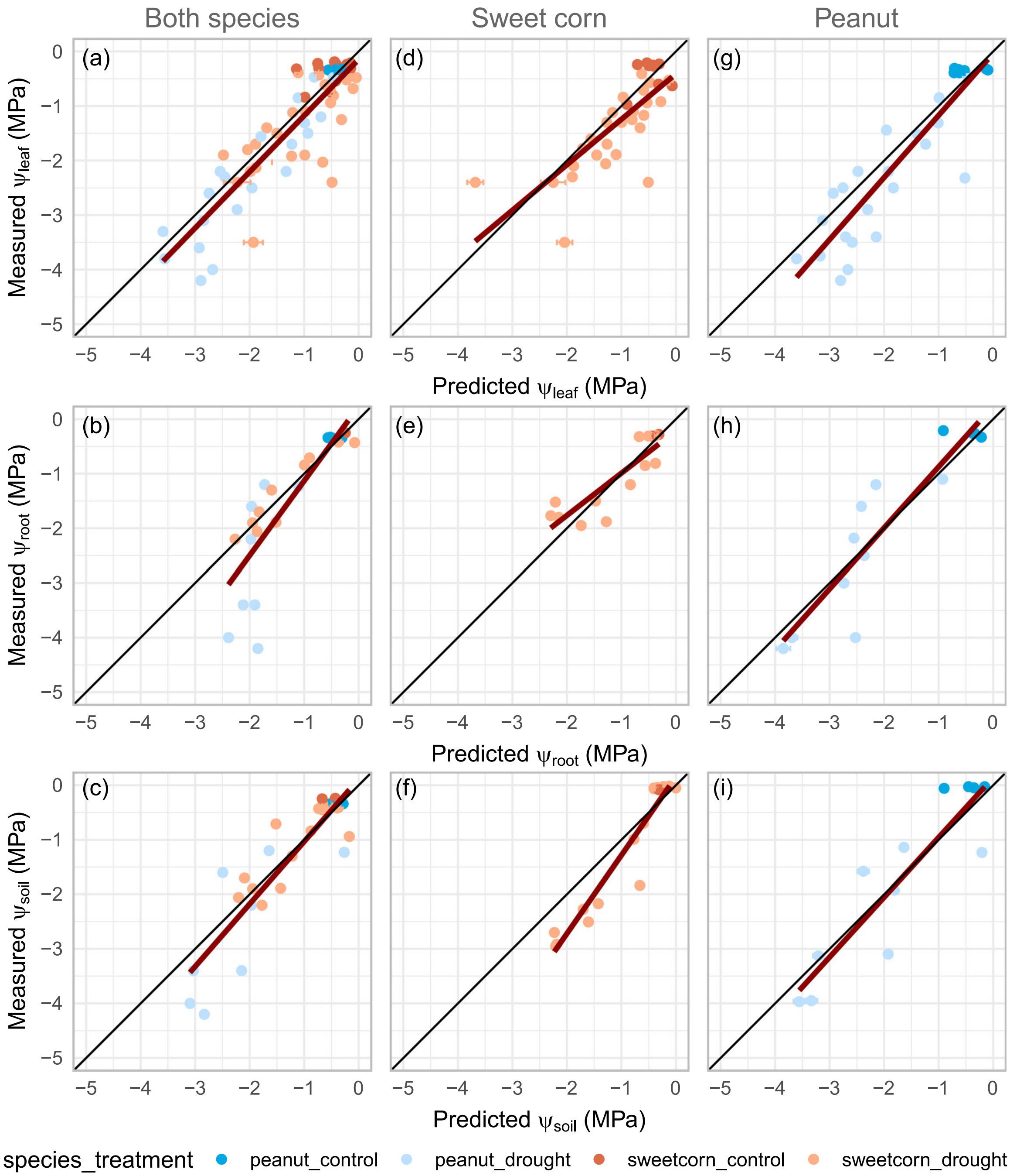

FIGURE 6 Plots of measured values against spectral reflectance (450–900 nm) predicted values using partial least square regression on external validation data sets for leaf water potential (Ψ_{leaf}), root water potential (Ψ_{root}) and soil water potential (Ψ_{soil}) of pooled species (a–c), sweet corn (d–f) and peanut (g–i). Dark blue (red) points are from control (well-watered) plants, and light blue (red) points are from peanut (sweet corn) plants under drought treatment. The black line is the 1:1 line. The red line indicates the line of best fit using ordinary least squares for each panel. We applied models generated from 100 iterations during training and testing to the corresponding spectral reflectance to get the 95% confidence intervals of each point. [Color figure can be viewed at wileyonlinelibrary.com]

insufficient to detect declining soil water status conditions in some species (Figure 7). Although we did not observe hydraulic segmentation between plant organs (Figure 4), it is important to acknowledge that if segmentation had happened via leaf or terminal branch shedding, it could influence the model's capacity to detect belowground processes from aboveground organs. Specifically, predicted root water potentials would likely be significantly lower than the true root water potential. Thus, quantifying the fine-scale spatial distribution of root and soil water status in a nondestructive way will require spectral imagers deployed into the rhizosphere. While our approach provides insight into the potential of hyperspectral prediction of root and rhizosphere water status, important challenges

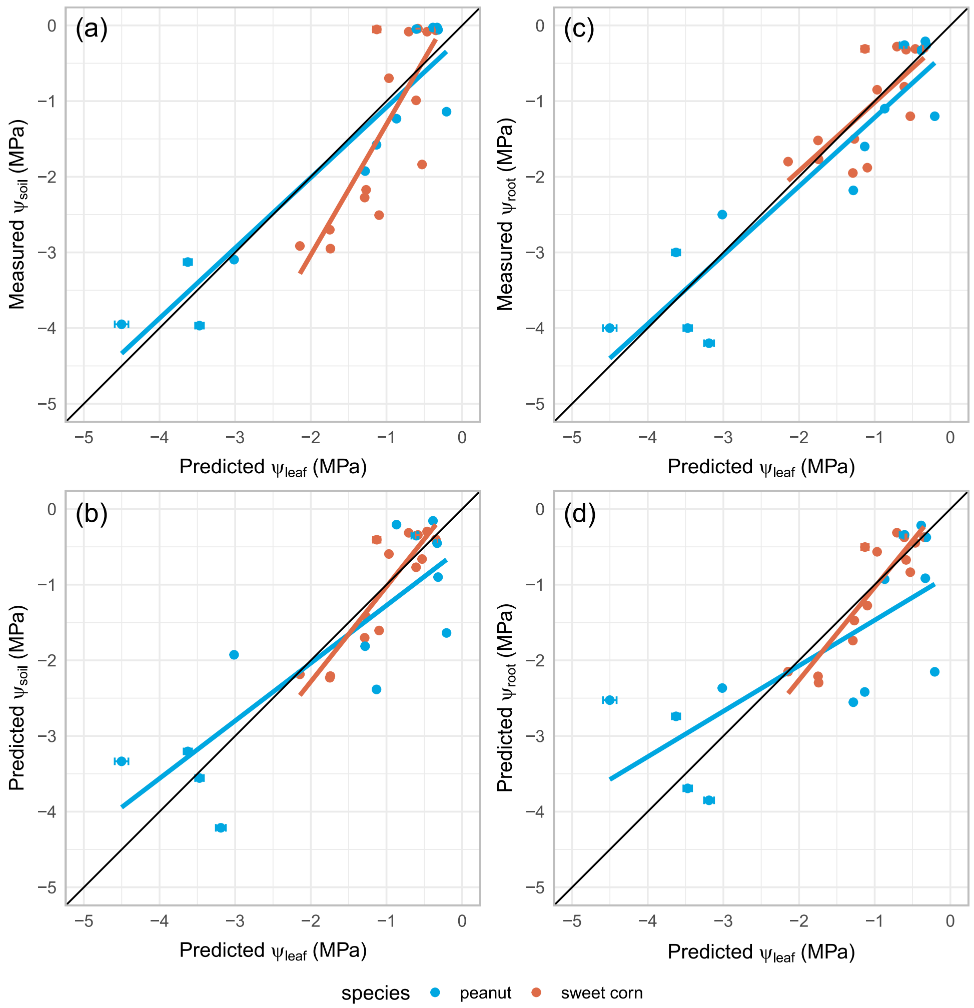

FIGURE 7 Plots of spectral reflectance (400–2400) predicted leaf potential (Ψ_{leaf}) against measured and spectral reflectance (450–900) predicted soil (Ψ_{soil}, a and b) and root (Ψ_{root}, c and d) water potentials. Estimating Ψ_{soil} based on reflectance estimates of Ψ_{leaf} in species that disconnect from the soil will overestimate Ψ_{soil} (a). Only species that maintain hydraulic continuity with the soil under drought hold a 1:1 relationship between Ψ_{soil} and Ψ_{leaf} that enables the prediction of soil water deficit based on canopy spectral reflectance (a). The black line is the 1:1 line. [Color figure can be viewed at wileyonlinelibrary.com]

and next steps remain. Here, we outline potential scenarios where soil–plant hydraulic disequilibrium may occur and provide a roadmap for research in hyperspectral imaging of the plant rhizosphere.

Soil–plant disequilibrium can result from plant strategies to maintain hydration or from soil characteristics. Our rhizoboxes were relatively small in volume, relative to the soil volume that both peanut and sweet corn are known to occupy under field conditions. While box volume restricted root growth compared to field conditions, the volume (of box and soil) was carefully controlled so that these effects would be even across all plants, still allowing our study to quantify hyperspectral signals in the soil for the first time. Notably, we observed declines in plant and soil water potential similar to what has been observed in previously published field studies (Bennett et al., 1981; Xu, 2001). Species like sweet corn might disconnect from dry soils (Figure 4) through reductions in aquaporin expression, root shrinkage, root hair death, suberization of cortical cells, cortical lacunae formation and mucilage exudate formation (Carminati, 2012; Cuneo et al., 2016; Duddek et al., 2022; Shekoofa & Sinclair, 2018) to avoid low water potentials and lethal levels of embolism (Duddek et al., 2022; North & Nobel, 1997). These processes can severely increase the hydraulic resistance of roots making it account for >95% of the whole-plant hydraulic continuum resistance in moderately water-stressed plants (Rodriguez-Dominguez & Brodribb, 2020) and minimize soil–plant flows. As such, soil water may have an easier time travelling from the soil to the atmosphere via evaporation than through a plant that has increased the soil-to-plant hydraulic resistance in response to drought stress, leading to increasingly different soil and plant water potentials over time. Alternatively, soil–root disconnection might occur due to the shrinkage of soil (Affortit et al., 2024; Cai et al., 2022), a process typical of clay-rich soils. Hydraulically disconnecting roots from the soil during severe drought may offer advantages during prolonged drought as they create a longer 'hydrated' phase for plants (Mackay et al., 2015; Nobel & Cui, 1992), effectively extending the time to hydraulic failure (Hammond & Adams, 2019). However, this disconnection comes as a recovery cost—it requires time and energy for plants to restore physiological functions, as shown in the relatively slower sweet corn recovery of photosynthetic capacity (F_v/F_m), which took at least 2 days longer to recover than peanut after rehydration. In contrast, species like peanut which maintain hydraulic connections with the surrounding soil (Figure 4), risk exposure to lethal water potentials. Maintaining hydraulic connection with the soil during severe droughts could be advantageous during short droughts as physiological recovery might be quicker relative to species that experience disequilibrium. Maintaining hydraulic connection might also be beneficial in plants highly resistant to embolism formation (i.e., low P_{50}) as they would experience minimal impact on plant function. Thus, we expect that although it has never been measured, *Arachis hypogaea* L. may be highly resistant to hydraulic failure, allowing plants to avoid hydraulic dysfunction while providing a means of rapid recovery. Notably, published values of P50 for *Zea mays* P50 are −1.2 MPa (Gleason et al., 2017), indicating that our observation of disequilibrium may evidence a hydraulic dysfunction avoidance strategy. While leveraging plant canopies as signal transducers for belowground processes have been previously proposed (Bagherian et al., 2023; Ramírez et al., 2023), we urge caution as sensing of rhizosphere water status through canopy spectra should thus be constrained to those species and soil conditions known to favour hydraulic continuity under drought (Figure 7).

It is critically important to identify the most informative wavelengths to predict water status across the soil–plant–atmosphere continuum. Present technologies aimed at imaging the rhizosphere are limited to monochrome or RGB imagery (Johnson et al., 2001; Xu et al., 2022). Given the current size and working distance of hyperspectral imagers, deploying this technology belowground in an unconstrained rooting zone is not yet possible. Thus, one of the most immediate future steps is identifying wavelengths suitable for the development of small, field-deployable multi- and hyperspectral imagers for further study of rhizosphere function (and dysfunction). In our study, we identified important wavelengths shared across models (Supporting Information S1: Figures 6 and 7; wavelengths 450–550, 650–750, 1500–1800 nm), while others appeared to be species-specific. Wavelengths at 500–550, 650–750 and 1500–1800 nm of the plant spectrum are associated with pigment content, stress conditions, photosynthetic activities and water content (Eitel et al., 2011; Ely et al., 2019; Peters & Noble, 2014). Their commonality across species and organs such as leaves and roots is thus expected due to their direct relationship to water status or to reduced pigment function caused by slow metabolism and increased oxidative stress when water is scarce. In the case of soil spectra, wavelengths 450–550 and 650–750 nm are associated with soil organic content (Conforti et al., 2018). In our case, specific wavelengths might be exclusive to our studied species or a feature of their differing drought response strategies. Exploring the extent to which wavelength importance may be associated with drought response strategy -as illustrated with peanut and sweet corn- should be a priority to resolve. Studies of buried rhizoboxes, and the development of small multispectral imagers capable of rhizosphere imaging, will help validate the use of these wavelengths and scale the approaches outlined here to less-restricted soil environments.

While we have revealed the potential for hyperspectral imaging to detect plant root and soil functional states, a diversity of other soil conditions needs to be similarly tested. The media used in our rhizoboxes (greens grade) was selected due to its homogeneity relative to most field soils. This simplification provided a more homogenous soil environment, with low organic matter and an even pore size. Our experiment's simplified media allowed us to unveil the potential for spectral mapping of rhizosphere water status, but future research should seek to understand its efficacy in soil environments of increasing complexity. Complex soils are rich and diverse in chemistry and structure, and roots share space with other organisms such as mycorrhiza and microbial communities (Zhou et al., 2022). Soil chemistry and structure, mycorrhiza and microbes all interact with plant roots in processes of water uptake and retention (Sangwan & Prasanna, 2022). Each of these elements has its own spectral signature. Sensing the identity and function of mycorrhiza, soil microbial communities and their functions, and developing diagnostics for soil characteristics might be possible through imagers capable of rhizosphere mapping. From a plant physiology perspective, future studies may also wish to explore the degree to which hydraulic continuity and disequilibrium are strategies more or less associated with plant photosynthetic pathways (e.g., C3, C4 or crassulacean acid metabolism). Stressors in the soil are similarly diverse; here, we have shown the potential for monitoring soil and plant root responses to drought stress, yet inundation (Lagomasino et al., 2021), saltwater intrusion (Middleton & David, 2022) and freezing stress (Prerostova et al., 2021) all routinely impact the rhizosphere environment and deserve further study.

5 | CONCLUSION

Our study provides the first evidence of the potential for hyper- and multispectral approaches to quantify not just structure, but function, in the rhizosphere in a nondestructive manner. These nondestructive measures of plant and soil water status have numerous applications, especially at the root–soil interface. Future studies that follow similar approaches should use less constrained rooting environments, which could also enable real-time study of root architecture and development in response to water deficit. Our modelling approach paves the way for future research to quantify root water status at a spatial scale not previously possible on intact plants. On our warming planet, plant water status is important for the many services that plants provide in natural and agricultural systems; being able to monitor these dynamic systems in a nondestructive way may provide numerous insights. Future work is needed to understand the additional rhizosphere processes to which our approach may be extended and the full potential of hyperspectral rhizosphere imaging for nondestructive detection of signals in the soil.

ACKNOWLEDGEMENTS

This research was supported by the US Department of Agriculture, National Institute of Food and Agriculture, Soil Health programme under accession no. 1024671. Funding was also provided by the Southeastern Peanut Research Initiative and Florida Peanut Producers Association.

DATA AVAILABILITY STATEMENT

The data that support the findings of this study are available from the corresponding author upon reasonable request.

ORCID

Yangyang Song http://orcid.org/0000-0002-4385-4538

REFERENCES

Affortit, P., Ahmed, M.A., Grondin, A., Delzon, S., Carminati, A. & Laplaze, L. (2024) Keep in touch: the soil–root hydraulic continuum and its role in drought resistance in crops. *Journal of Experimental Botany*, 75, 584–593. Available from: https://doi.org/10.1093/jxb/erad312

Alizadeh, M.R., Adamowski, J., Nikoo, M.R., AghaKouchak, A., Dennison, P. & Sadegh, M. (2020) A century of observations reveals increasing likelihood of continental-scale compound dry-hot extremes. *Science Advances*, 6(39), eaaz4571. Available from: https://doi.org/10.1126/sciadv.aaz4571

Babaeian, E., Homaee, M., Vereecken, H., Montzka, C., Norouzi, A.A. & van Genuchten, M.T. (2015) A comparative study of multiple approaches for predicting the soil–water retention curve: hyperspectral information vs. basic soil properties. *Soil Science Society of America Journal*, 79(4), 1043–1058. Available from: https://doi.org/10.2136/sssaj2014.09.0355

Bagherian, K., Bidese-Puhl, R., Bao, Y., Zhang, Q., Sanz-Saez, A., Dang, P.M. et al. (2023) Phenotyping agronomic and physiological traits in peanut under mid-season drought stress using UAV-based hyperspectral imaging and machine learning. *The Plant Phenome Journal*, 6(1), e20081. Available from: https://doi.org/10.1002/ppj2.20081

Bangelesa, F., Adam, E., Knight, J., Dhau, I., Ramudzuli, M. & Mokotjomela, T.M. (2020) Predicting soil organic carbon content using hyperspectral remote sensing in a degraded mountain landscape in Lesotho. *Applied and Environmental Soil Science*, 2020, 1–11. Available from: https://doi.org/10.1155/2020/2158573

Bartlett, M.K., Scoffoni, C., Ardy, R., Zhang, Y., Sun, S., Cao, K. et al. (2012) Rapid determination of comparative drought tolerance traits: using an osmometer to predict turgor loss point. *Methods in Ecology and Evolution*, 3(5), 880–888. Available from: https://doi.org/10.1111/j.2041-210X.2012.00230.x

Bennett, J.M., Boote, K.J. & Hammond, L.C. (1981) Alterations in the components of peanut leaf water potential during desiccation. *Journal of Experimental Botany*, 32(130), 1035–1043.

Bitterlich, M., Sandmann, M. & Graefe, J. (2018) Arbuscular mycorrhiza alleviates restrictions to substrate water flow and delays transpiration limitation to stronger drought in tomato. *Frontiers in Plant Science*, 9, 154. Available from:https://doi.org/10.3389/fpls.2018.00154

Blackburn, G.A. (2007) Hyperspectral remote sensing of plant pigments. *Journal of Experimental Botany*, 58(4), 855–867. Available from: https://doi.org/10.1093/jxb/erl123

Bodner, G., Nakhforoosh, A., Arnold, T. & Leitner, D. (2018) Hyperspectral imaging: a novel approach for plant root phenotyping. *Plant Methods*, 14(1), 84. Available from: https://doi.org/10.1186/s13007-018-0352-1

Le Bot, J., Serra, V., Fabre, J., Draye, X., Adamowicz, S. & Pagès, L. (2010) DART: a software to analyse root system architecture and development from captured images. *Plant and Soil*, 326(1), 261–273. Available from: https://doi.org/10.1007/s11104-009-0005-2

Boyer, J.S., James, R.A., Munns, R., Condon, T.A.G. & Passioura, J.B. (2008) Osmotic adjustment leads to anomalously low estimates of relative water content in wheat and barley. *Functional Plant Biology*, 35(11), 1172–1182. Available from: https://doi.org/10.1071/FP08157

Bucci, S.J., Goldstein, G., Meinzer, F.C., Franco, A.C., Campanello, P. & Scholz, F.G. (2004) Mechanisms contributing to seasonal homeostasis of minimum leaf water potential and predawn disequilibrium between soil and plant water potential in Neotropical savanna trees. *Trees*, 19(3), 296–304. Available from https://doi.org/10.1007/s00468-004-0391-2

Cai, G., Ahmed, M.A., Abdalla, M. & Carminati, A. (2022) Root hydraulic phenotypes impacting water uptake in drying soils. *Plant, Cell & Environment*, 45(3), 650–663. Available from: https://doi.org/10.1111/pce.14259

Carminati, A. (2012) A model of root water uptake coupled with rhizosphere dynamics. *Vadose Zone Journal*, 11(3), vzj2011–0106. Available from: https://doi.org/10.2136/vzj2011.0106

Castillo-Argaez, R., Sapes, G., Mallen, N., Lippert, A., John, G.P., Zare, A. et al. (2024) Spectral ecophysiology: hyperspectral pressure–volume curves to estimate leaf turgor loss. *New Phytologist*, 242, 935–946. Available from: https://doi.org/10.1111/nph.19669

Cavender-Bares, J., Sack, L. & Savage, J. (2007) Atmospheric and soil drought reduce nocturnal conductance in live oaks. *Tree Physiology*, 27(4), 611–620. Available from: https://doi.org/10.1093/treephys/27.4.611

Chang, S.J., Chowdhry, R., Song, Y., Mejia, T., Hampton, A. & Kucharski, S. et al. (2023) HyperPRI: a dataset of hyperspectral images for underground plant root study. *bioRxiv*. Available from: https://doi.org/10.1101/2023.09.29.559614

Cohen, Y., Alchanatis, V., Zusman, Y., Dar, Z., Bonfil, D.J., Karnieli, A. et al. (2010) Leaf nitrogen estimation in potato based on spectral data and on simulated bands of the VENμS satellite. *Precision Agriculture*, 11(5), 520–537. Available from: https://doi.org/10.1007/s11119-009-9147-8

Conforti, M., Matteucci, G. & Buttafuoco, G. (2018) Using laboratory Vis-NIR spectroscopy for monitoring some forest soil properties. *Journal of Soils and Sediments*, 18(3), 1009–1019. Available from: https://doi.org/10.1007/s11368-017-1766-5

Cuneo, I.F., Knipfer, T., Brodersen, C.R. & McElrone, A.J. (2016) Mechanical failure of fine root cortical cells initiates plant hydraulic decline during drought. *Plant Physiology*, 172(3), 1669–1678. Available from: https://doi.org/10.1104/pp.16.00923

Donovan, L.A., Grisé, D.J., West, J.B., Pappert, R.A., Alder, N.N. & Richards, J.H. (1999) Predawn disequilibrium between plant and soil water potentials in two cold-desert shrubs. *Oecologia*, 120(2), 209–217. Available from: https://doi.org/10.1007/s004420050850

Donovan, L., Linton, M. & Richards, J. (2001) Predawn plant water potential does not necessarily equilibrate with soil water potential under well-watered conditions. *Oecologia*, 129(3), 328–335. Available from: https://doi.org/10.1007/s004420100738

Donovan, L.A., Richards, J.H. & Linton, M.J. (2003) Magnitude and mechanisms of disequilibrium between predawn plant and soil water potentials. *Ecology*, 84(2), 463–470. Available from: https://doi.org/10.1890/0012-9658(2003)084[0463:MAMODB]2.0.CO;2

Duddek, P., Carminati, A., Koebernick, N., Ohmann, L., Lovric, G., Delzon, S. et al. (2022) The impact of drought-induced root and root hair shrinkage on root–soil contact. *Plant Physiology*, 189(3), 1232–1236. Available from: https://doi.org/10.1093/plphys/kiac144

Dwivedi, S.L., Siddique, K.H.M., Farooq, M., Thornton, P.K. & Ortiz, R. (2018) Using biotechnology-led approaches to uplift cereal and food legume yields in dryland environments. *Frontiers in Plant Science*, 9, 1249. Available from: https://doi.org/10.3389/fpls.2018.01249

Eitel, J.U.H., Vierling, L.A., Litvak, M.E., Long, D.S., Schulthess, U., Ager, A.A. et al. (2011) Broadband, red-edge information from satellites improves early stress detection in a New Mexico conifer woodland. *Remote Sensing of Environment*, 115(12), 3640–3646. Available from: https://doi.org/10.1016/j.rse.2011.09.002

Elfving, D.C., Kaufmann, M.R. & Hall, A.E. (1972) Interpreting leaf water potential measurements with a model of the soil-plant-atmosphere continuum. *Physiologia Plantarum*, 27(2), 161–168. Available from: https://doi.org/10.1111/j.1399-3054.1972.tb03594.x

Ely, K.S., Burnett, A.C., Lieberman-Cribbin, W., Serbin, S.P. & Rogers, A. (2019) Spectroscopy can predict key leaf traits associated with source–sink balance and carbon–nitrogen status. *Journal of Experimental Botany*, 70(6), 1789–1799. Available from: https://doi.org/10.1093/jxb/erz061

Fàbregas, N. & Fernie, A.R. (2019) The metabolic response to drought. *Journal of Experimental Botany*, 70(4), 1077–1085. Available from: https://doi.org/10.1093/jxb/ery437

Féret, J.-B., le Maire, G., Jay, S., Berveiller, D., Bendoula, R., Hmimina, G. et al. (2019) Estimating leaf mass per area and equivalent water thickness based on leaf optical properties: potential and limitations of physical modeling and machine learning. *Remote Sensing of Environment*, 231, 110959. Available from: https://doi.org/10.1016/j.rse.2018.11.002

Gleason, S.M., Wiggans, D.R., Bliss, C.A., Comas, L.H., Cooper, M., DeJonge, K.C. et al. (2017) Coordinated decline in photosynthesis and hydraulic conductance during drought stress in *Zea mays*. *Flora*, 227, 1–9. Available from: https://doi.org/10.1016/j.flora.2016.11.017

Gloaguen, R.M., Brym, Z.T., Peeples, J., Xu, W., Chun, H.-C. & Rowland, D.L. (2022) The plasticity of early root development in *Sesamum indicum* L. as influenced by genotype, water, and nutrient availability. *Rhizosphere*, 21, 100457. Available from: https://doi.org/10.1016/j.rhisph.2021.100457

Gloaguen, R.M., Couch, A., Rowland, D.L., Bennett, J., Hochmuth, G., Langham, D.R. et al. (2019) Root life history of non-dehiscent sesame (*Sesamum indicum* L.) cultivars and the relationship with canopy development. *Field Crops Research*, 241, 107560. Available from: https://doi.org/10.1016/j.fcr.2019.107560

Grieco, M., Schmidt, M., Warnemünde, S., Backhaus, A., Klück, H.-C., Garibay, A. et al. (2022) Dynamics and genetic regulation of leaf nutrient concentration in barley based on hyperspectral imaging and machine learning. *Plant Science*, 315, 111123. Available from: https://doi.org/10.1016/j.plantsci.2021.111123

Groenveld, T., Obiero, C., Yu, Y., Flury, M. & Keller, M. (2023) Predawn leaf water potential of grapevines is not necessarily a good proxy for soil moisture. *BMC Plant Biology*, 23, 369. Available from: https://doi.org/10.21203/rs.3.rs-2795033/v1

Guadagno, C.R., Ewers, B.E., Speckman, H.N., Aston, T.L., Huhn, B.J., DeVore, S.B. et al. (2017) Dead or alive? Using membrane failure and chlorophyll a fluorescence to predict plant mortality from drought. *Plant Physiology*, 175(1), 223–234. Available from: https://doi.org/10.1104/pp.16.00581

Guo, P., Li, T., Gao, H., Chen, X., Cui, Y. & Huang, Y. (2021) Evaluating calibration and spectral variable selection methods for predicting three soil nutrients using Vis-NIR spectroscopy. *Remote Sensing*, 13(19), 4000. Available from: https://doi.org/10.3390/rs13194000

Gupta, A., Rico-Medina, A. & Caño-Delgado, A.I. (2020) The physiology of plant responses to drought. *Science*, 368(6488), 266–269. Available from: https://doi.org/10.1126/science.aaz7614

Haber-Pohlmeier, S., Tötzke, C., Lehmann, E., Kardjilov, N., Pohlmeier, A. & Oswald, S.E (2019) Combination of magnetic resonance imaging and neutron computed tomography for three-dimensional rhizosphere imaging. *Vadose Zone Journal*, 18(1), 1–11. Available from: https://doi.org/10.2136/vzj2018.09.0166

Hammond, W.M. & Adams, H.D. (2019) Dying on time: traits influencing the dynamics of tree mortality risk from drought. *Tree Physiology*, 39(6), 906–909. Available from: https://doi.org/10.1093/treephys/tpz050

Hammond, W.M., Williams, A.P., Abatzoglou, J.T., Adams, H.D., Klein, T., López, R. et al. (2022) Global field observations of tree die-off reveal hotter-drought fingerprint for Earth's forests. *Nature Communications*, 13, 1761. Available from: https://doi.org/10.1038/s41467-022-29289-2

Hammond, W.M., Yu, K., Wilson, L.A., Will, R.E., Anderegg, W.R.L. & Adams, H.D. (2019) Dead or dying? Quantifying the point of no return from hydraulic failure in drought-induced tree mortality. *New Phytologist*, 223(4), 1834–1843. Available from: https://doi.org/10.1111/nph.15922

Hanavan, R.P., Pontius, J. & Hallett, R. (2015) A 10-Year assessment of hemlock decline in the catskill mountain region of New York State using hyperspectral remote sensing techniques. *Journal of Economic Entomology*, 108(1), 339–349. Available from: https://doi.org/10.1093/jee/tou015

Ihuoma, S.O. & Madramootoo, C.A. (2019) Sensitivity of spectral vegetation indices for monitoring water stress in tomato plants. *Computers and Electronics in Agriculture*, 163, 104860. Available from: https://doi.org/10.1016/j.compag.2019.104860

Johnson, M.G., Tingey, D.T., Phillips, D.L. & Storm, M.J. (2001) Advancing fine root research with minirhizotrons. *Environmental and Experimental Botany*, 45(3), 263–289. Available from: https://doi.org/10.1016/S0098-8472(01)00077-6

Lagomasino, D., Fatoyinbo, T., Castañeda-Moya, E., Cook, B.D., Montesano, P.M., Neigh, C. et al. (2021) Storm surge and ponding explain mangrove dieback in southwest Florida following Hurricane Irma. *Nature Communications*, 12, 4003. Available from: https://doi.org/10.1038/s41467-021-24253-y

Legg, S. (2021) IPCC, 2021: climate change 2021—the physical science basis. *Interaction*, 49, 44–45. Available from: https://doi.org/10.3316/informit.315096509383738

Li, X., Blackman, C.J., Peters, J.M.R., Choat, B., Rymer, P.D., Medlyn, B.E. et al. (2019) More than iso/anisohydry: hydroscapes integrate plant water use and drought tolerance traits in 10 eucalypt species from contrasting climates. *Functional Ecology*, 33(6), 1035–1049. Available from: https://doi.org/10.1111/1365-2435.13320

Ma, S., Zhou, Y., Gowda, P.H., Dong, J., Zhang, G., Kakani, V.G. et al. (2019) Application of the water-related spectral reflectance indices: a review. *Ecological indicators*, 98, 68–79. Available from: https://doi.org/10.1016/j.ecolind.2018.10.049

Mackay, D.S., Roberts, D.E., Ewers, B.E., Sperry, J.S., McDowell, N.G. & Pockman, W.T. (2015) Interdependence of chronic hydraulic dysfunction and canopy processes can improve integrated models of tree response to drought. *Water Resources Research*, 51(8), 6156–6176. Available from: https://doi.org/10.1002/2015WR017244

Martin-StPaul, N., Delzon, S. & Cochard, H. (2017) Plant resistance to drought depends on timely stomatal closure. *Ecology Letters*, 20(11), 1437–1447. Available from https://doi.org/10.1111/ele.12851

Martinez-Vilalta, J., Anderegg, W.R.L., Sapes, G. & Sala, A. (2019) Greater focus on water pools may improve our ability to understand and anticipate drought-induced mortality in plants. *New Phytologist*, 223(1), 22–32. Available from https://doi.org/10.1111/nph.15644

McDowell, N.G., Sapes, G., Pivovaroff, A., Adams, H.D., Allen, C.D. & Anderegg, W.R.L. et al. (2022) Mechanisms of woody-plant mortality under rising drought, CO_2 and vapour pressure deficit. *Nature Reviews*

Earth & Environment, 3(5), 1–15. Available from: https://doi.org/10.1038/s43017-022-00272-1

Michaletz, S.T. (2018) Xylem dysfunction in fires: towards a hydraulic theory of plant responses to multiple disturbance stressors. *New Phytologist*, 217(4), 1391–1393. Available from: https://doi.org/10.1111/nph.15013

Mickelbart, M.V., Hasegawa, P.M. & Bailey-Serres, J. (2015) Genetic mechanisms of abiotic stress tolerance that translate to crop yield stability. *Nature Reviews Genetics*, 16(4), 237–251. Available from: https://doi.org/10.1038/nrg3901

Middleton, B.A. & David, J.L. (2022) Trends in vegetation and height of the topographic surface in a tidal freshwater swamp experiencing rooting zone saltwater intrusion. *Ecological Indicators*, 145, 109637. Available from: https://doi.org/10.1016/j.ecolind.2022.109637

Narisetti, N., Henke, M., Seiler, C., Junker, A., Ostermann, J., Altmann, T. et al. (2021) Fully-automated root image analysis (faRIA). *Scientific Reports*, 11(1), 16047. Available from: https://doi.org/10.1038/s41598-021-95480-y

Nobel, P.S. & Cui, M. (1992) Hydraulic conductances of the soil, the root-soil air gap, and the root: changes for desert succulents in drying soil. *Journal of Experimental Botany*, 43(3), 319–326. Available from: https://doi.org/10.1093/jxb/43.3.319

North, G.B. & Nobel, P.S. (1997) Root-soil contact for the desert succulent *Agave deserti* in wet and drying soil. *New Phytologist*, 135(1), 21–29. Available from: https://doi.org/10.1046/j.1469-8137.1997.00620.x

Peters, R.D. & Noble, S.D. (2014) Spectrographic measurement of plant pigments from 300 to 800 nm. *Remote Sensing of Environment*, 148, 119–123. Available from: https://doi.org/10.1016/j.rse.2014.03.020

Pflugfelder, D., Metzner, R., van Dusschoten, D., Reichel, R., Jahnke, S. & Koller, R. (2017) Non-invasive imaging of plant roots in different soils using magnetic resonance imaging (MRI. *Plant Methods*, 13(1), 102. Available from: https://doi.org/10.1186/s13007-017-0252-9

Prerostova, S., Zupkova, B., Petrik, I., Simura, J., Nasinec, I., Kopecky, D. et al. (2021) Hormonal responses associated with acclimation to freezing stress in *Lolium perenne*. *Environmental and Experimental Botany*, 182, 104295. Available from: https://doi.org/10.1016/j.envexpbot.2020.104295

R Core Team. (2020) *R: A language and environment for statistical computing*. R Foundation for Statistical Computing. Available from: https://www.r-project.org/

Ramírez, D.A., Grüneberg, W., I Andrade, M., De Boeck, B., Loayza, H., S Makunde, G. et al. (2023) Phenotyping of productivity and resilience in sweetpotato under water stress through UAV-based multispectral and thermal imagery in Mozambique. *Journal of Agronomy and Crop Science*, 209(1), 41–55. Available from: https://doi.org/10.1111/jac.12565

Reynolds, J.F., Smith, D.M.S., Lambin, E.F., Turner, B.L., Mortimore, M., Batterbury, S.P.J. et al. (2007) Global desertification: building a science for dryland development. *Science*, 316(5826), 847–851. Available from: https://doi.org/10.1126/science.1131634

Rodriguez-Dominguez, C.M. & Brodribb, T.J. (2020) Declining root water transport drives stomatal closure in olive under moderate water stress. *New Phytologist*, 225(1), 126–134. Available from: https://doi.org/10.1111/nph.16177

Rodriguez-Dominguez, C.M., Forner, A., Martorell, S., Choat, B., Lopez, R., Peters, J. et al. (2022) Leaf water potential measurements using the pressure chamber: synthetic testing of assumptions towards best practices for precision and accuracy. *Plant, Cell & Environment*, 45(7), 2037–2061. Available from: https://doi.org/10.1111/pce.14330

Sack, L., John, G.P. & Buckley, T.N. (2018) ABA accumulation in dehydrating leaves is associated with decline in cell volume, not turgor pressure. *Plant Physiology*, 176(1), 489–495. Available from: https://doi.org/10.1104/pp.17.01097

Samuelson, L.J., Pell, C.J., Stokes, T.A., Bartkowiak, S.M., Akers, M.K., Kane, M. et al. (2014) Two-year throughfall and fertilization effects on leaf physiology and growth of loblolly pine in the Georgia Piedmont. *Forest Ecology and Management*, 330, 29–37. Available from: https://doi.org/10.1016/j.foreco.2014.06.030

Sangwan, S. & Prasanna, R. (2022) Mycorrhizae helper bacteria: unlocking their potential as bioenhancers of plant–arbuscular mycorrhizal fungal associations. *Microbial Ecology*, 84(1), 1–10. Available from: https://doi.org/10.1007/s00248-021-01831-7

Sapes, G., Schroeder, L., Scott, A., Clark, I., Juzwik, J., Montgomery, R.A. et al. (2024) Mechanistic links between physiology and spectral reflectance enable previsual detection of oak wilt and drought stress. *Proceedings of the National Academy of Sciences of the United States of America*, 121(7), e2316164121. Available from: https://doi.org/10.1073/pnas.2316164121

Scholz, F.G., Bucci, S.J., Goldstein, G., Meinzer, F.C., Franco, A.C. & Miralles-Wilhelm, F. (2007) Biophysical properties and functional significance of stem water storage tissues in Neotropical savanna trees. *Plant, Cell & Environment*, 30(2), 236–248. Available from: https://doi.org/10.1111/j.1365-3040.2006.01623.x

Scoffoni, C. & Sack, L. (2017) The causes and consequences of leaf hydraulic decline with dehydration. *Journal of Experimental Botany*, 68(16), 4479–4496. Available from: https://doi.org/10.1093/jxb/erx252

Shekoofa, A. & Sinclair, T.R. (2018) Aquaporin activity to improve crop drought tolerance. *Cells*, 7(9), 123. Available from: https://doi.org/10.3390/cells7090123

Shen, C, Liu, L., Zhu, L., Kang, J., Wang, N. & Shao, L. (2020) High-throughput in situ root image segmentation based on the improved DeepLabv3+ method. *Frontiers in Plant Science*, 11, 576791. Available from: https://doi.org/10.3389/fpls.2020.576791

Song, Y., Tseng, Y., Rowland, D.L., Tillman, B.L., Wilson, C.H., Sarnoski, P.J. et al. (2021) Multiple-generation seed maturity effects on seedling vigour in a production environment. *Journal of Agronomy and Crop Science*, 207(6), 1024–1040. Available from: https://doi.org/10.1111/jac.12559

Tillman, B.L. & Gorbet, D.W. (2017) Registration of 'TUFRunner '511" peanut. *Journal of Plant Registrations*, 11(3), 235–239. Available from: https://doi.org/10.3198/jpr2016.11.0064crc

Tomasella, M., Calderan, A., Mihelčič, A., Petruzzellis, F., Braidotti, R. & Natale, S. et al. (2023) Best procedures for leaf and stem water potential measurements in grapevine: cultivar and water status matter. *Plants*, 12(13), 2412. Available from: https://doi.org/10.3390/plants12132412

Whalley, W.R., Ober, E.S. & Jenkins, M. (2013) Measurement of the matric potential of soil water in the rhizosphere. *Journal of Experimental Botany*, 64(13), 3951–3963. Available from: https://doi.org/10.1093/jxb/ert044

Wolfe, B.T., Sperry, J.S. & Kursar, T.A. (2016) Does leaf shedding protect stems from cavitation during seasonal droughts? A test of the hydraulic fuse hypothesis. *New Phytologist*, 212(4), 1007–1018. Available from: https://doi.org/10.1111/nph.14087

Xu, H.-L. (2001) Soil-root interface water potential in sweet corn as affected by organic fertilizer and a microbial inoculant. *Journal of Crop Production*, 3(1), 139–156. Available from: https://doi.org/10.1300/J144v03n01_13

Xu, C., Qu, J.J., Hao, X., Cosh, M.H., Zhu, Z. & Gutenberg, L. (2020) Monitoring crop water content for corn and soybean fields through data fusion of MODIS and Landsat measurements in Iowa. *Agricultural Water Management*, 227, 105844. Available from: https://doi.org/10.1016/j.agwat.2019.105844

Xu, W., Yu, G., Cui, Y., Gloaguen, R., Zare, A. & Bonnette, J. et al. (2022) PRMI: a dataset of minirhizotron images for diverse plant root study. *arXiv*. http://arxiv.org/abs/2201.08002

Zhou, J., Zhang, L., Feng, G. & George, T.S. (2022) Arbuscular mycorrhizal fungi have a greater role than root hairs of maize for priming the rhizosphere microbial community and enhancing rhizosphere organic P mineralization. *Soil Biology and Biochemistry*, 171, 108713. Available from: https://doi.org/10.1016/j.soilbio.2022.108713

Zurweller, B.A., Rowland, D.L., Tillman, B.L., Payton, P., Migliaccio, K., Wright, D. et al. (2018) Assessing above- and below-ground traits of disparate peanut genotypes for determining adaptability to soil hydrologic conditions. *Field Crops Research*, 219, 98–105. Available from: https://doi.org/10.1016/j.fcr.2018.01.020

Zwieniecki, M.A., Brodribb, T.J. & Holbrook, N.M. (2007) Hydraulic design of leaves: insights from rehydration kinetics. *Plant, Cell & Environment*, 30(8), 910–921. Available from: https://doi.org/10.1111/j.1365-3040.2007.001681.x

SUPPORTING INFORMATION

Additional supporting information can be found online in the Supporting Information section at the end of this article.

How to cite this article: Song, Y., Sapes, G., Chang, S., Chowdhry, R., Mejia, T., Hampton, A. et al. (2024) Hyperspectral signals in the soil: Plant–soil hydraulic connection and disequilibrium as mechanisms of drought tolerance and rapid recovery. *Plant, Cell & Environment*, 1–17. https://doi.org/10.1111/pce.15011